PNAS RESEARCH ARTICLE | EARTH, ATMOSPHERIC, AND PLANETARY SCIENCES

Phanerozoic flooding of North America and the Great Unconformity

Adrian R. Tasistro-Hart[a,1] and Francis A. Macdonald[a]

Edited by Michael Manga, University of California, Berkeley, München, Germany; received May 30, 2023; accepted August 2, 2023

The flooding record of North America has been used to infer patterns of global erosion and sea level in deep time. Here, we utilize the geospatial dimension of the stratigraphic record provided by the Macrostrat database, and patterns of erosion from thermochronology, to resolve local tectonic subsidence from global sea level. We show that the flooding history of North America correlates in space and time with continent-facing subduction along active margins, consistent with subduction-driven dynamic topographic subsidence of the continental interior. Nonetheless, the continentally aggregated flooding signal of North America is an exaggerated global M-curve of Phanerozoic sea level. This coincidence relates to the closing of the geodynamic loop of the supercontinent cycle: Subduction under North America accommodated both the makeup and breakup of Pangaea, which, coupled with changing ridge length, flattened hypsometry, and increased sea level both locally and globally. The sole Phanerozoic exception to this pattern of global sea level tracking North American near-field geodynamics is the Cambrian Sauk transgression. We argue that this is a far-field record of the inception of circum-Gondwanan subduction, independent of North America, which significantly flattened Earth's hypsometry. This hypsometric flattening displaced ocean water globally, flooding tectonically passive North America to seal the Great Unconformity.

sea level | Great Unconformity | dynamic topography | macrostratigraphy

Significance

Marine sediments across North America record multiple flooding events over the Phanerozoic, starting with the Sauk Transgression that seals the Great Unconformity. Using Macrostrat, a geospatial database of stratigraphy, we demonstrate that these flooding events, except the Sauk, correspond temporally and spatially with subduction under North America, consistent with near-field dynamic subsidence. We suggest that the Sauk resulted from the migration of subduction zones from oceanic to continental arcs around Gondwana, which flattened global hypsometry and displaced ocean water onto North America. Our analysis links the Phanerozoic flooding of North America to local and global tectonics and suggests that sea level is set by the amount of oceanic spreading that is balanced by subduction under continental relative to oceanic lithosphere.

The stratigraphic record of North America has been used to infer global sea level (1, 2), erosion (3), and sedimentary preservation through deep time (4). These sea level–modulated sedimentary fluxes are commonly depicted as the first-order control on geochemical cycles and atmospheric oxygen (5) and have been interpreted as a boundary condition for complex life (6). Yet, the Phanerozoic marine flooding of ancestral North America, or Laurentia, recorded at a continental scale by the Sloss sequences, is a spatially and temporally heterogeneous signal (7). The Sloss sequences, which track six to seven continental-scale transgressions, have motivated hypotheses for eustatic (1, 8, 9) or dynamic topographic (10–12) control of continental flooding. Due to the inextricable link between geodynamics and sea level via global hypsometry, these often competing hypotheses amount to two sides of the same coin. However, distinguishing between these forcings is critical for quantitatively reconstructing global budgets from local records and determining the geophysical drivers for particular flooding episodes, like the transgressive sequence above the Great Unconformity.

The globally averaged rate of oceanic spreading is frequently portrayed as the dominant control on long-term global sea level (eustasy). A longer total ridge length, or faster-spreading ridges, generates more young, warm, and therefore buoyant oceanic lithosphere, elevating ocean basins and displacing sea water onto continents (13). This Pitman model of sea level, however, must conserve mass: If ocean basins go up, then some other part of Earth's surface must go down (14). From this perspective, if elevated oceanic lithosphere in one part of the globe is entirely compensated by subsiding oceanic lithosphere elsewhere, then the net effect on sea level is zero. Increased spreading rates must be complemented by a geodynamic mechanism for subsiding land masses above sea level in order to increase sea level (14) (Fig. 1). An obvious candidate for this geodynamic coupling is subduction along continental margins, which can cause dynamic subsidence of continental lithosphere above descending slabs (10). A slab subducting under continental lithosphere, creating a continental arc, can contribute to both local and global sea level rise, whereas a slab subducting under oceanic crust, creating an oceanic arc, cannot.

This geodynamic framework motivates the "hypsometric see-saw" of ref. 14, which provides a simple model that couples oceanic and continental elevation perturbations (Fig. 1). Uplift of oceanic elevations is compensated by subsidence of continental

Author affiliations: [a]Department of Earth Science, Webb Hall, University of California, Santa Barbara, CA 93106

Author contributions: A.R.T.-H. and F.A.M. designed research; A.R.T.-H. performed research; A.R.T.-H. analyzed data; and A.R.T.-H. and F.A.M. wrote the paper.

The authors declare no competing interest.

This article is a PNAS Direct Submission.

[1]To whom correspondence may be addressed. Email: adrian@tasistro-hart.com.

This article contains supporting information online at https://www.pnas.org/lookup/suppl/doi:10.1073/pnas.2309084120/-/DCSupplemental.

Published September 5, 2023.

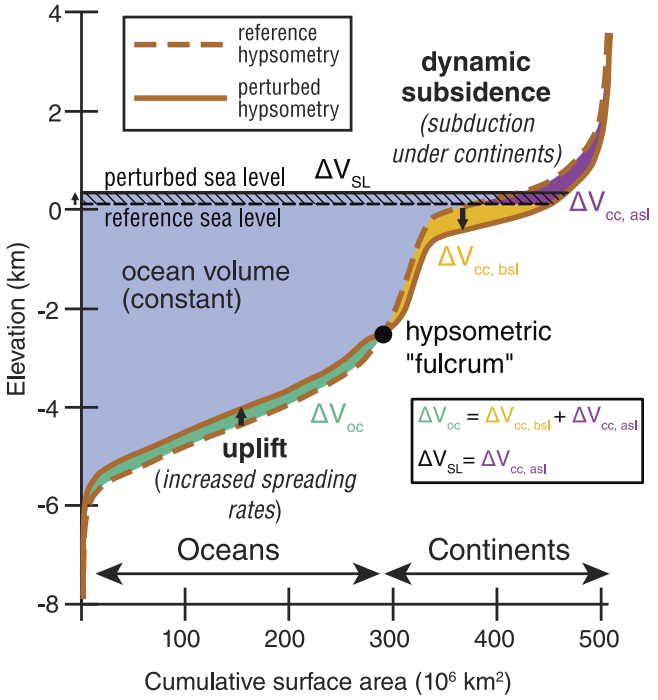

Fig. 1. Schematic model of global hypsometry as a dynamic "see-saw" modified from ref. 14. Elevations are either oceanic or continental, and uplift in one domain is compensated by subsidence in the other about a "hypsometric fulcrum" at the transition between oceans and continents, which is the mean depth of ocean spreading ridges (2.6 km). The perturbation illustrated in the figure (dashed brown line to solid brown line) shows uplift of oceanic elevations resulting from increased spreading rates, which is compensated by subsidence of continents over subducting slabs. This compensation preserves mass such that $\Delta V_{oc} = \Delta V_{cc,bsl} + \Delta V_{cc,asl}$. ΔV_{oc} is the displaced volume in the oceanic realm, and $\Delta V_{cc,bsl}$ and $\Delta V_{cc,asl}$ are the compensating volumes in the continental realm below and above the unperturbed sea level, respectively. This hypsometric perturbation both increases flooding area (the intersection of sea level with hypsometry) and the elevation of sea level itself. Sea level elevation increases such that $\Delta V_{sl} = \Delta V_{cc,asl}$, where ΔV_{sl} is the hatched area, which is the globally displaced ocean water volume that matches the uplifted volume oceanic not balanced by subsidence of submerged continental volumes.

elevations (and vice versa) to conserve mass. The elevation for the hypsometric fulcrum about which the compensation occurs is −2600 m, which is the average elevation of mid-ocean ridges. While this model clearly oversimplifies global geodynamic complexity, it does provide a useful near upper bound on the amplitude of sea level variability by constraining all elevation perturbations in the ocean basins to be compensated by elevation perturbations in the continents.* This model highlights the importance of subduction under continents for generating a eustatic effect via hypsometric flattening. If seafloor spreading was entirely compensated by oceanic arcs, the hypsometric effect would be almost entirely in the oceanic realm, yielding negligible impact on eustasy. That is, an Earth dominated by oceanic arcs would have relatively low sea level compared to one dominated by continental arcs.

This simple hypsometric model yields two separate contributions to continental flooding. The first is dynamic subsidence from subduction along an active margin. The second is the eustatic effect from the displaced volume of the oceans associated with oceanic spreading (ΔV_{SL} in Fig. 1). However, there is a mismatch in the spatial scale of near-field effects of dynamic subsidence from subduction, and the far-field effects of eustasy: Subduction drives subsidence on length scales of 100s of kms, whereas large continents are 1,000s of kms across (Fig. 2). Thus, instead of averaging flooding area at the continental scale, a spatial analysis of the geometry of flooding is necessary to untangle near-field subsidence from far-field eustasy.

*It is only near an upper bound because sea level variability would be even greater for a model whose hypsometric fulcrum was around 0 km elevation.

Macrostrat

Since Sloss's seminal work (7), new datasets of continental sedimentation have emerged (15–17), among them Macrostrat (4), which provides a spatially resolved database of continental sedimentation. Macrostrat has been previously used to estimate the spatially aggregated sedimentary coverage of Laurentia through time (18, 19), which has fueled arguments ranging from sedimentary periodicity (20) to oxygenation of Earth's atmosphere (5). This spatially aggregated time series of sedimentation has been put forth both as a signal of primary sediment preservation (18) and as a signal of continental erosion across the Great Unconformity (3), with the stepwise increase in Phanerozoic sediment abundance—the Sauk sequence—providing the locus of these contradictory interpretations (Fig. 3). The geospatial dimension of Macrostrat, however, has remained underutilized.

Macrostrat organizes geology into units that are bound to geospatial columns, which form an irregular polygonal dissection of North America (4). All units are defined by beginning and end ages, and sedimentary units are tagged with inferred depositional environments. To investigate the record of continental flooding, we consider only marine sedimentary units: a Macrostrat column is considered "flooded" if it contains marine sedimentary units in a given time window (Fig. 2). As past workers have also done (5, 20), we work with the presence or absence of sedimentary units, and we use the areas of Macrostrat columns to quantify flooding extent. While Macrostrat units include minimum and maximum thickness estimates, which could add a further dimension for geospatial flooding analysis, we find that these thicknesses are not useful at the subcontinental length scales and million-year time scales of our analysis (*SI Appendix*).

As a first-order investigation of the spatial structure of continental sedimentation, we compute the area fractional coverage by marine sediments of Laurentia within spatial windows expanding from the continental interior outward toward the margins (Fig. 3). This computation is done with 10 My time windows, and we define the continental boundary as the cratonic perimeter of Laurentia (corrected for the rifting of Greenland). The rationale for this analysis is to evaluate how the Sloss sequences record flooding of the interior versus the margin. Far-field eustatic flooding should encroach from the margin inward, while regional dynamic subsidence should have a more complicated spatial flooding signature that may be stronger in the interior of the continent and along active margins.

Results

The spatially windowed time series of Laurentian flooding area resolve the Sloss sequences as areal flooding peaks (Fig. 3*A*). These flooding peaks are slightly enhanced in the Mesozoic and mid-Paleozoic by the reincorporation of eroded sedimentary cover (*SI Appendix*). This effect is small, however, consistent with previous interpretations that the Phanerozoic sedimentary cover of North America is primarily a signal of preservation (19, 23). Five flooding events, each <50 My in duration, are well resolved and correspond to the Sauk, Tippecanoe, Kaskaskia I, Zuni I,

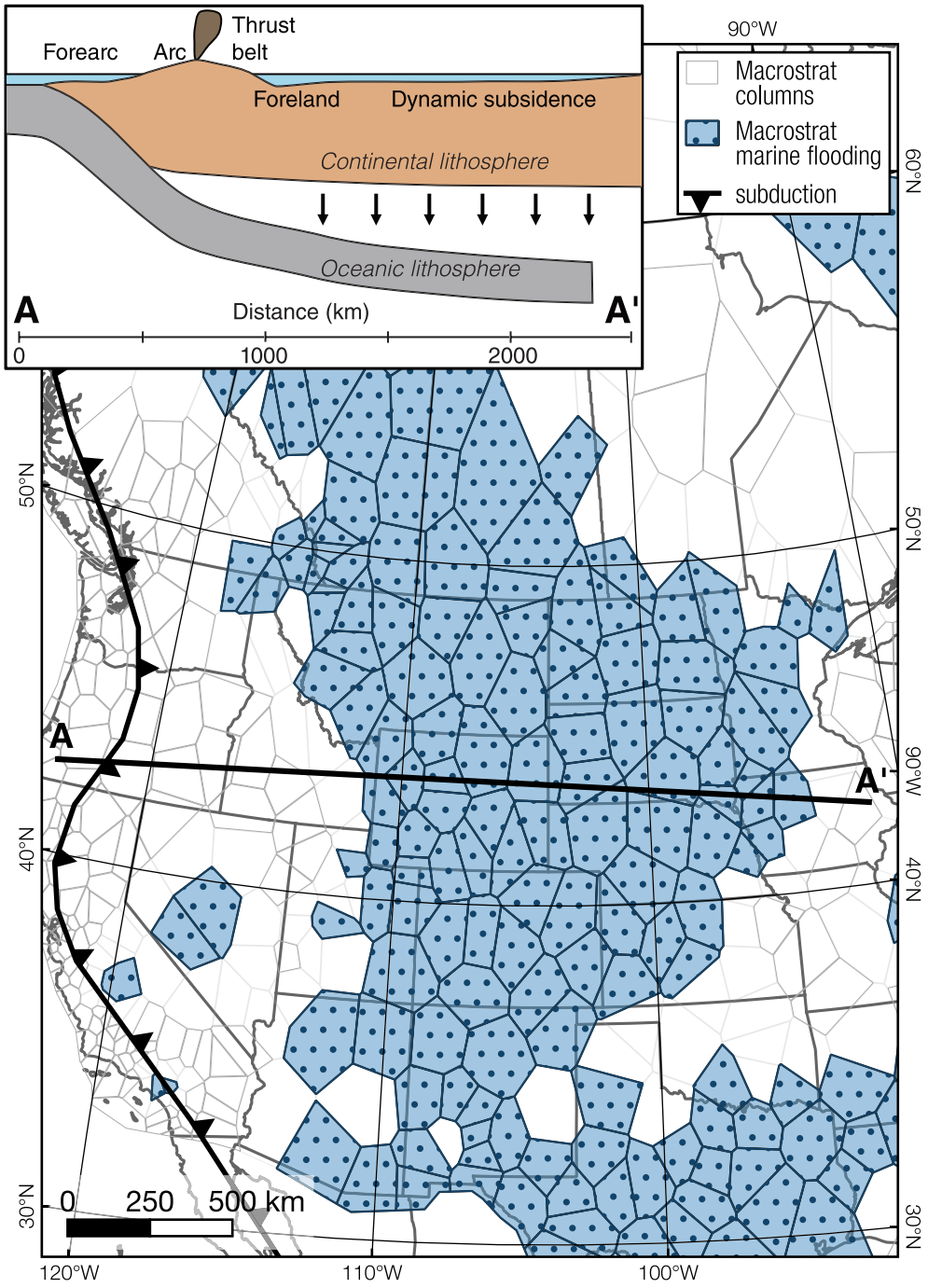

Fig. 2. Marine sedimentation in the Late Cretaceous Western Interior Basin. Macrostrat columns containing marine sediments over the time interval 120 to 80 Ma are shown with blue stippled fills. All Macrostrat columns are shown in light gray. The inset shows the cross-section of Farallon subduction under North America (21, 22), illustrating the tectonic components of the subduction system and the vertically exaggerated dynamic subsidence resulting from subduction along the transect A-A′.

and Zuni II sequences. All flooding peaks are strongest when accounting for the entire area of the continent (i.e., interior and margin), but how flooding area changes with distance from the continental interior varies significantly by Sloss sequence. The Sauk Transgression provides one end-member, where fractional flooding area monotonically increases as progressively more continental area is included, expanding from the interior to the margin. The Tippecanoe sequence, on the other hand, provides another end-member, exhibiting essentially constant fractional flooding area regardless of how much of the continent interior or margin is considered. In general, the Zuni I, II, and Kaskaskia I flooding peaks obtain the area fractional flooding observed over the entire continent within several hundred kilometers of the margin, indicating that the flooding signal is driven by large swaths of the continental interior. Only the Sauk sequence appears to be clearly driven by flooding progressing from the margin toward the interior (Fig. 3*B*).

The spatial maps corresponding to each flooding peak reveal the footprint of each Sloss sequence. The Sauk transgression involves almost the entire perimeter of Laurentia but is most

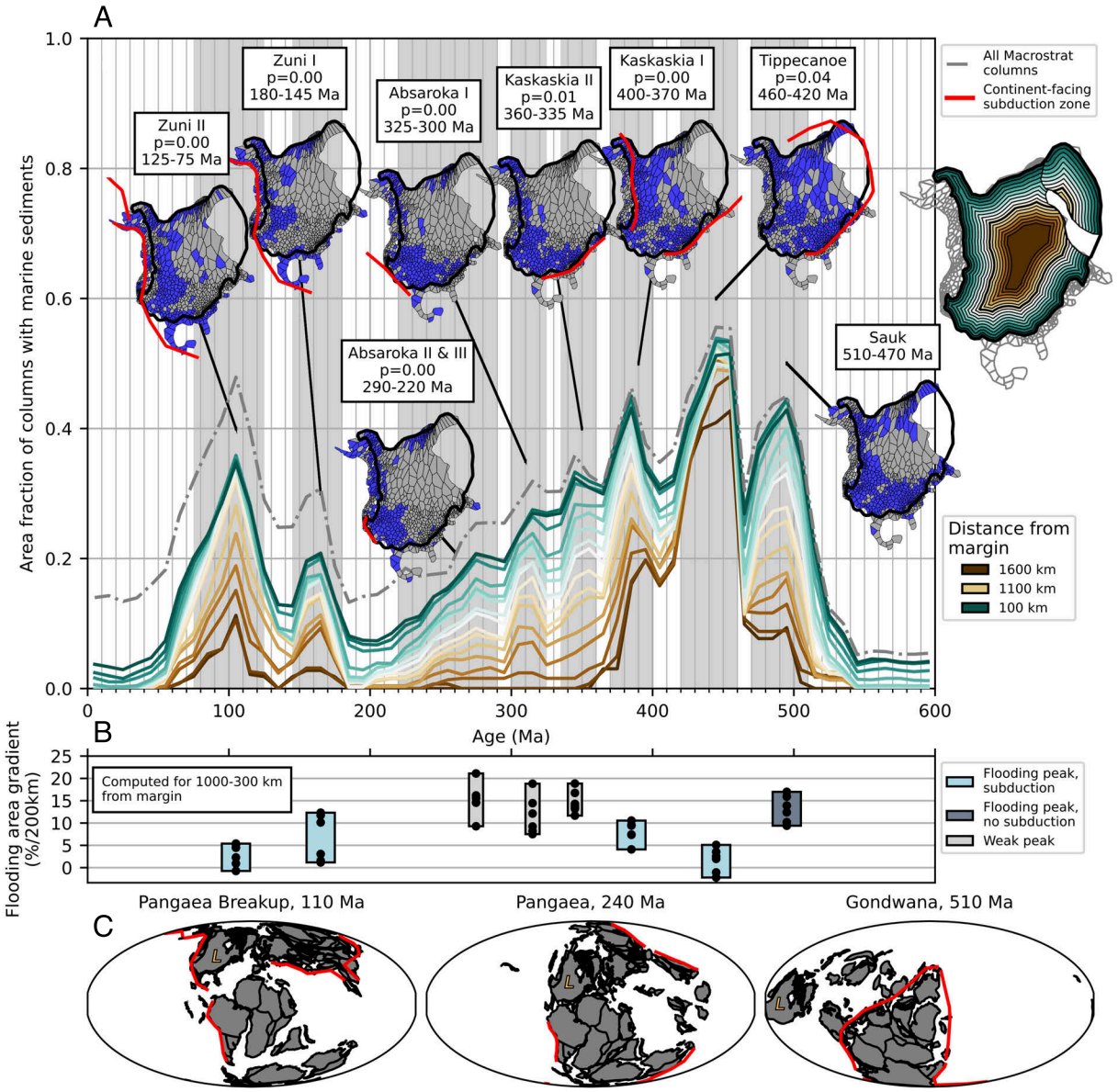

Fig. 3. (*A*) Laurentian continental area fraction coverage of marine sediments through the Phanerozoic. Area fraction is computed within spatially buffered areas, expanding outward from the continental interior (brown) to the margin (green). Area fraction for all North American Macrostrat columns is shown as the gray dashed line. Spatial distributions of marine sediments are shown as snapshots for the prominent flooding peaks: a Macrostrat column is colored blue if it contains marine sediments at any time within the time window. Continental facing subduction zone traces are also shown for each time window. The *P* values for Sloss sequences associated with active margins refer to the statistical test for association of flooding with subduction geometry (*SI Appendix*, Fig. S5). (*B*) Flooding area gradients for each Sloss sequence. Gradients are computed as the increase in area fraction flooded from the interior to the margin, normalized by the maximum flooded area, and taken as a percentage. The gradients (shown as black dots) are computed over 200 km increments from 1,000 to 300 km from the margin. These gradients effectively show the spacing between the lines in (*A*). Low values indicate that area flooding fraction does not change from the interior toward the margin, while high values indicate that flooding increases toward the margin. (*C*) Three snapshots show global paleogeography from ref. 66. Continental-dipping subduction zone traces are also plotted for these time snapshots. North America is labeled with an "L".

pronounced in southern Laurentia, where marine carbonates formed as far north as Wisconsin. The Tippecanoe and Kaskasia I peaks are largely driven by sedimentation along the eastern and north–northwestern portions of Laurentia but also involve significant flooding of the continental interior in the Williston, Hudson Bay, Michigan, and Illinois cratonic basins (24). Flooded area then decreases through the Carboniferous to the end Triassic during the formation of Pangaea, with marine sedimentation moving south and west during deposition in the mid-continent Permian Basin. Marine flooding then increases with the Zuni I and II sequences in the Jurassic and Cretaceous, respectively, which occur along the western flank of the continent. In summary, Macrostrat records the spatial heterogeneity of the Sloss sequences, showing the time-varying footprints of continental flooding.

Extrapolation of Laurentian flooding area to global flooding area broadly replicates the shape of the M-curve of Phanerozoic eustasy reported by numerous other studies (Fig. 4). The M-curve shows peaks of sea level in the early Paleozoic and late Mesozoic, with lows in the early Mesozoic and Cenozoic. Agreement is strongest with the two other flooding-based eustatic reconstructions of refs. 25 and 26. Individual second-order flooding peaks, however, do not correlate across records. Nevertheless, the broad congruence between Laurentian flooding and global sea level

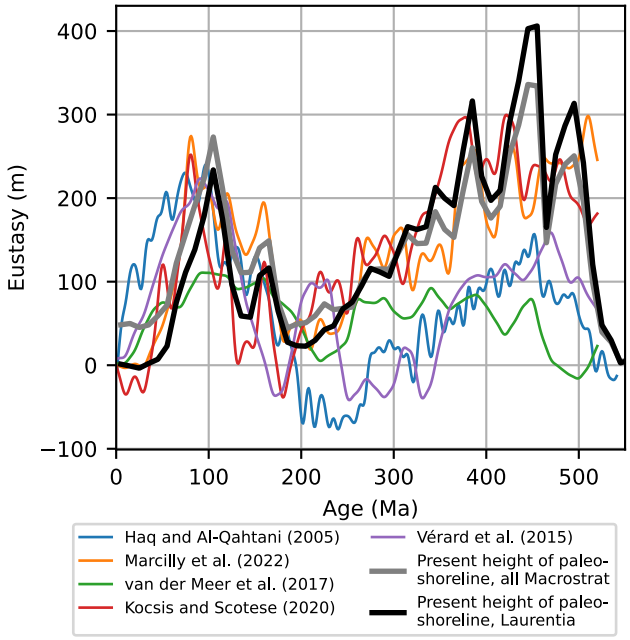

Fig. 4. Estimates of global sea level. The black curve is constructed by extrapolating Laurentian flooding area to global flooding area and onto sea level via the hypsometric model of ref. 14. The gray curve shows the same procedure but with all North American Macrostrat data. The reconstructions from refs. 26 and 25 are also based on continental flooding areas. All records (except the Macrostrat curves) are smoothed for easier visualization by lowpass filtering with a digital Butterworth filter with a 5-My critical frequency.

seems paradoxical given the aforementioned spatial heterogeneity that constitutes the continental flooding signal.

Subduction-Driven Continental Flooding

With the exception of the Sauk transgression, each well-defined flooding peak corresponds to a period of continent-facing subduction along convergent margins (Fig. 3). We develop a statistic to quantitatively evaluate the significance of the spatial distribution of flooding with respect to subduction zone geometry (*SI Appendix*, Figs. S5 and S6). Two separate tests utilizing this statistic demonstrate the close association of sedimentation with subduction zone geometry for these flooding peaks (*SI Appendix*). Furthermore, in each case, the wavelength of the flooded continental area is far greater than typical foreland basin widths on the order of <500 km (e.g., ref. 27), suggesting the role of dynamic subsidence driven by subduction (28). We develop this concept by describing the tectonic setting of Laurentia during each of the non-Sauk flooding peaks and linking it to the observed geometry of marine flooding, as well as existing geodynamic models.

The Tippecanoe peak, from 460 to 420 Ma, coincides with the Salinic orogeny and the initiation of west-dipping subduction along the eastern margin of Laurentia after collision of the Taconic arcs above an east-dipping slab, slab-breakoff, and reversal (29, 30). This subduction possibly wrapped around northern Laurentia (31). Ref. 32 modeled cratonic sedimentation in response to continent-facing 470 to 430 Ma subduction along eastern Laurentia and broadly reproduced the observed sedimentation pattern in eastern Laurentia. Subduction along northern Laurentia provides a dynamic mechanism for the marine flooding observed in northern Laurentia. Reactivation of subsidence in intracratonic basins has also been linked to the dynamic effects of subduction (33).

The Kaskaskia I peak is largely driven by widespread marine sedimentation along the northwestern margin of Laurentia, which coincided with east-dipping Late Devonian subduction along northwestern Laurentia (34–37). The dynamic response to activation of this margin has been modeled by ref. 38, who reproduced the extent of Devonian subsidence and sedimentation in response to subduction. By the end Late Devonian, slab retreat (34, 36, 39) or oblique convergence (40) coincides with the marked cessation of marine sedimentation around northwest Laurentia and the end of the Kaskaskia I peak.

The Kaskaskia I peak also records sedimentation along southeastern Laurentia, which is typically interpreted as the upper plate during Devonian convergence (e.g., ref. 41), consistent with continental arc magmatism during the Famennian event (42). The cessation of widespread marine sedimentation in northeastern Laurentia is consistent with Early Devonian collision with the Amorican Spur, which moved subduction outboard of the continent and flipped its polarity (43). Other tectonic models, however, instead interpret southward subduction with Laurentia as the lower plate during closure of the Rheic Ocean (44). We argue that the geometry of sedimentation is more consistent with subduction dipping under Laurentia and dynamic subsidence of the continental interior.

During the final assembly of Pangaea, total marine flooding of Laurentia decreases, and the locus of sedimentation shifts to southwestern Laurentia. A small peak corresponding to the Kaskaskia II sequence includes continued marine flooding of southeastern Laurentia during subduction and final closure of the Rheic Ocean. The Absaroka I and II sequences, which do not constitute strong flooding peaks, mainly record the Late Paleozoic flooding of southwestern Laurentia associated with foreland basin formation (45), and arc magmatism in the Mojave (46, 47), providing evidence for continent-facing subduction along at least some of southwestern Laurentia. The Absaroka sequences additionally include the onset of thermal subsidence in the Sverdrup Basin along the passive northern margin of Laurentia (48), exhibiting sedimentation over a much shorter length scale.

The final two flooding peaks correspond to the Zuni sequences, which track the formation of the Sundance Seaway and Western Interior Basin. Substantial geodynamic modeling and basin analysis has linked subsidence of the continent, especially during the Cretaceous, to the dynamic effects of Farallon subduction (12, 32, 49, 50). The Zuni I peak of the Sundance Seaway begins with the initiation of Farallon subduction, and the long wavelength of marine sedimentation has previously been interpreted as filling dynamic accommodation (51, 52). A lull in marine sedimentation occurs from roughly 145 to 130 Ma, which corresponds to an interpreted decrease in convergence rates potentially related to a more steeply subducting slab (22). The resumption of increased convergence rates and shallowing slab subduction results in the Zuni II sequence, with flooding area peaking around 100 Ma (Fig. 2). After 100 Ma, flooded area decreases as the Farallon slab eventually flattened and slowed with eastward migration (22, 53), ultimately stagnating and rolling back.

Sea Level

The preceding discussion has argued for the primarily regional, Laurentian geodynamic origin of the continent's flooding to explain its heterogeneous spatial distribution. Yet, extrapolation of Laurentian to global continental flooding area and then eustasy via the simple hypsometric model of ref. 14 (*SI Appendix*)

broadly replicates other eustatic reconstructions (Fig. 4). Eustasy extrapolated from Laurentian flooding agrees particularly well with the reconstructions of refs. 26 and 25, which are both based on global coastline compilations. This congruence between flooding area-based sea level estimations reinforces the first-order nature of the M-curve for global Phanerozoic sea level. This interpretation means that some amount of the flooding of Laurentia is due to hypsometric perturbations originating elsewhere on the globe. Simultaneously, Laurentian geodynamics participate in hypsometric perturbations that drive global sea level variability: Dynamic subsidence of North America flattens global hypsometry, contributing to a global flooding signal (Fig. 1).

While the record of Laurentian flooding broadly reproduces the global M-curve of Phanerozoic sea level, individual flooding peaks in the record have different relationships with the M-curve. For example, the Tippecanoe sequence extrapolated globally suggests an additional 100 to 200 m of sea level increase in the Late Ordovician. We do not suggest that this is actually the case but just point out that this flooding event represents a Laurentia-specific excursion from the M-curve, demonstrating more intense subsidence of the continent relative to the rest of the continents. The relatively amplified subsidence of Laurentia at this time is consistent with it being a global locus of continent-dipping subduction (54). On the other hand, the Zuni I sequence neatly matches Late Jurassic flooding peaks from the records of both refs. (26) and 25. This correlation is consistent with subduction of Tethyan and Pacific lithosphere accommodating the break up of Pangaea (54, 55), which affected many continental margins (Fig. 3*C*). The diachronous Permian to Triassic sea level low in these records coincides with the assembly of Pangaea and migration of subduction zones away from major continents to the Central-Asian orogenic belt, as displayed by abundant ophiolites and sutures with continental ribbons of this age (56).

The Great Unconformity as a Far-Field Record of Hypsometric Flattening

The Great Unconformity on North America is defined below by Archean to Neoproterozoic rocks and above by the Sauk Transgression. Recent thermochronology studies have demonstrated that erosion below the Great Unconformity is diachronous across North America (57–59) and includes multiple overlapping unconformities (60). These unconformities developed with the Stenian to early Tonian (ca. 1100 to 900 Ma) assembly of Rodinia (57), followed by late Tonian to Cryogenian breakup (800 to 635 Ma) (59). The unifying feature of the Great Unconformity on North America is then the Sauk Transgression, which predominantly covers it. We now present a model for the Sauk Transgression, which is the remaining Sloss Sequence that demands accounting.

The Sauk Transgression peaks from 500 to 490 Ma. During this time, Laurentia is relatively tectonically quiescent, without active subduction on any margin, and yet flooding occurs synchronously along almost all margins. Flooding is also strongest closer to the margins, decreasing in fractional coverage toward the continental interior (Fig. 3*B*), suggestive of a eustatic origin. The eastern and southern margins of North America preserve Ediacaran–Cambrian rift–drift transitions that account for some of the local subsidence along these margins (61) and likely exaggerate this signal, but evidence for Ediacaran to Cambrian rifting on the northern and western margins is less clear. Particularly along the western margin of Laurentia, the Sauk sequence is frequently interpreted as recording the onset of thermal subsidence following the end of protracted

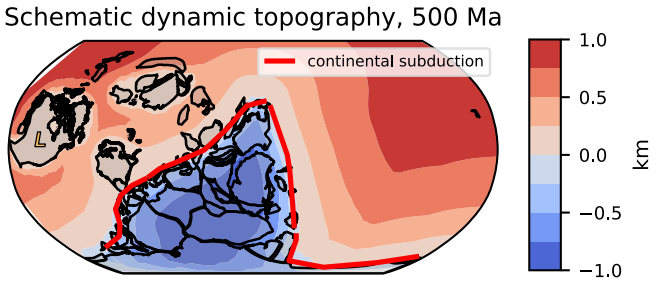

Fig. 5. Schematic representation of global dynamic topography in response to circum-Gondwana subduction compensating oceanic spreading: Red is positive, and blue is negative. The schematic replicates output from geodynamic modeling by ref. 67 with the paleogeography from ref. 66.

Cryogenian rifting (62–64). This mismatch in subsidence models between Cryogenian rifting and extensive sedimentation peaking over 135 My later can be reconciled by accounting for a large Cambrian sea level rise (65). We argue that the broad extent of flooding that characterizes the Sauk Transgression, with carbonates extending all the way to Wisconsin, cannot be explained by thermal subsidence alone.

We propose that the Sauk Transgression occurred in response to the transfer of subduction zones from the oceanic realm to continental arcs in circum-Gondwanan subduction. This continental subduction caused dynamic subsidence of much of the Gondwanan interior, compensating a net increase in the elevation of oceanic lithosphere (Fig. 5). The resultant hypsometric flattening displaced ocean water globally, including onto Laurentia, thereby providing the eustatic mechanism for sealing the Great Unconformity.

Rodinia to Gondwana. North America formed the core of Rodinia (68). During Rodinia breakup, North America was likely situated in an upwelling zone analogous to Mesozoic–Cenozoic Africa (69–71), as evidenced by several Neoproterozoic LIPs (61). North America was then relatively elevated while rifting occurred along all of its margins (68, 72). The new spreading zones were compensated by increased subduction taken up largely in the oceanic realm, as recorded by the pulse of ophiolite generation in the Arabian–Nubian Shield (73), the Saharides (74, 75), the Brasilides (76), and the Altaids (77). In contrast, there are few preserved extensive Late Tonian to Cryogenian continental arcs along the major continents (54). This abundance of subduction in oceanic arcs relative to that under the continents should have led to a global hypsometric steepening and relatively low sea level, compounding the localized effect of upwelling under North America. This Neoproterozoic tectonic history explains the dearth of marine sediments across North America over the course of the Rodinia supercontinent cycle.

Tonian to Cryogenian ophiolite generation during subduction initiation in the oceanic realm was followed by oceanic subduction that culminated in Cryogenian to Cambrian arc-continent collisions and terrane accretion around Gondwana, as exemplified in the obduction of vast oceanic tracts with ophiolites in the Arabian–Nubian Shield and Saharides (73, 74). By the Cambrian, extensive subduction developed under the continents that had assembled Gondwana, increasing the relative abundance of subduction in continental arcs adjacent to large land masses relative to oceanic arcs separated from the continents. In this framework, hypsometric flattening is responsible for the great flooding event that defines the Great Unconformity.

Abundant evidence exists for circum-Gondwanan subduction. The southern margin of Gondwana, spanning approximately 15,000 km, had initiated subduction by 530 Ma, which progressed into the Terra Australis Orogen that peaked around 515 to 500 Ma (78–82). The margin of northeastern Gondwana was also convergent within this time window, with subduction along the entire margin from Australia to Turkey from 530 to 490 Ma (82–85). This subduction extended west as part of the Avalonian-Cadomian orogenic arc, essentially along the entire northern margin of Gondwana (86–89). At 510 Ma, almost the entire perimeter of Gondwana—approximately 35,000 km—was experiencing continent-facing subduction evidenced by continental arc magmatism. This arc length is nearly twice that reported by ref. 54 at 510 Ma in their compilation of arc lengths and is comparable to their maximum Phanerozoic continental arc length reported during the Cretaceous. The abundance of ca. 510 Ma continental arc magmatism associated with the formation of Gondwana is also apparent in detrital zircon and zircon chemistry records, which show a peak in preserved zircon and negative ϵHf values associated with melt extraction from the upper plate in continental arcs (90).

The global dynamic topographic response to this subduction has been shown by the mantle convection model of ref. 67, who demonstrate the kilometer scale subsidence over the entirety of Gondwana and complementary topographic highs concentrated in the proto-Tethys and proto-Pacific Oceans. Although ref. 67 do not show flooding of North America at 520 to 480 Ma in their C1 reconstruction (their Fig. 4), this is a product of the assumptions in the plate reconstruction, whereas the M21 reconstruction produces strong far-field flooding (their Fig. 9). This result is precisely the hypsometric see-saw by which enhanced continental subduction lowers the continents and is balanced by enhanced seafloor spreading that raises the oceanic lithosphere, raising sea level globally and driving the Sauk Transgression.

Conclusions

The Phanerozoic stepwise increase in sediment preservation on North America is a first-order feature in Macrostrat mirrored in global estimates of sediment preservation, and it marks a dramatic departure from Neoproterozoic continental sedimentation (19, 91). Our argument linking the Phanerozoic flooding of North America, including the Sauk Transgression and the Great Unconformity, to the local and global distribution of subduction under continents provides a previously lacking geodynamic grounding. This new link reconciles the relative roles of near-field tectonic basin formation and far-field geodynamics on the distribution of the rich stratigraphic record that crowns North America.

Dynamic and tectonic subsidence are often treated independently from global sea level. Using Macrostrat, we suggest that they are connected through the hypsometric see-saw (14). In particular, the spatial dimension of Macrostrat allows us to link North American flooding events to episodes of continent-facing subduction, which participate in and superimpose on the Phanerozoic M-curve of eustasy. Thus, our analysis distinguishes near-field and far-field sea-level perturbations and highlights the power of spatially resolved sedimentary and tectonic datasets. Refinements to plate reconstructions coupled with dynamic topography models, along with development of spatial flooding datasets on continents besides North America, will provide future tests of our model.

Materials and Methods

We downloaded Macrostrat units and columns as geojson files via the v2 API. Our analysis reflects the state of the database in June 2023. Prior to analysis, we modified the Macrostrat database to account for new geochronologic age constraints for the Tapeats Sandstone with results from refs. 92 and 93. We also account for sediment erosion histories constrained by recent thermochronology on the Canadian Shield, using results from studies with time–temperature modeling that well constrains both Phanerozoic burial and exhumation (59, 94–97) (*SI Appendix*, Fig. S7). These studies reveal extensive Paleozoic burial, and, at least on the Slave Craton, Mesozoic exhumation and reburial followed by Cenozoic exhumation. It is possible that much of the shield experienced some degree of Paleozoic burial (98), but existing thermochronology only resolves some of this burial. Finally, we removed Quaternary marine units, whose interpretability is complicated by the hypsometric effects of Quaternary glaciations (*SI Appendix*, Fig. S9).

We also create maps of marine sedimentary coverage within time windows corresponding to the flooding peaks, which we assign to Sloss sequences based on temporal overlap (Fig. 3). These maps show Macrostrat columns that contain marine sediments at any time within the time window, visualizing the footprint of flooding extent during a Sloss sequence. For each Sloss sequence associated with continent-facing subduction, i.e., all but the Sauk, we evaluate the statistical significance of the flooding proximity to the active margin(s) against the null hypothesis of uniformly random flooding. For these tests, we define a geospatial statistic ζ (*SI Appendix*).

Finally, we extrapolate Laurentian flooding area to global flooding area and then to sea level using the simple parametric model of ref. 14 to compare with other global sea level records (Fig. 4). By performing this extrapolation, we only seek to model what a sea-level curve would look like if Laurentian flooding were representative of global flooding; we do not argue that it is.

Data, Materials, and Software Availability. Data and analysis are available in a GitHub repository https://doi.org/10.5281/zenodo.8148642.

ACKNOWLEDGMENTS. We acknowledge funding from NSF SedPaleo grant to FAM #1916698. We also acknowledge B. Flowers for helpful discussions. We thank our reviewers for constructive comments that greatly improved the manuscript.

1. B. U. Haq, J. Hardenbol, P. R. Vail, Chronology of fluctuating sea levels since the Triassic. *Science* **235**, 1156–1167 (1987).
2. B. U. Haq, S. R. Schutter, A chronology of Paleozoic sea-level changes. *Science* **322**, 64–68 (2008).
3. C. B. Keller *et al*., Neoproterozoic glacial origin of the Great Unconformity. *Proc. Natl. Acad. Sci. U.S.A.* **116**, 1136–1145 (2019).
4. S. E. Peters, J. M. Husson, J. Czaplewski, Macrostrat: A platform for geological data integration and deep-time earth crust research. *Geochem. Geophys. Geosyst.* **19**, 1393–1409 (2018).
5. J. M. Husson, S. E. Peters, Atmospheric oxygenation driven by unsteady growth of the continental sedimentary reservoir. *Earth Planetary Sci. Lett.* **460**, 68–75 (2017).
6. S. E. Peters, R. R. Gaines, Formation of the 'Great Unconformity' as a trigger for the Cambrian explosion. *Nature* **484**, 363–366 (2012).
7. L. L. Sloss, Sequences in the Cratonic interior of North America. *Geol. Soc. Am. Bull.* **74**, 93 (1963).
8. J. D. Hays, W. C. Pitman, Lithospheric plate motion, sea level changes and climatic and ecological consequences. *Nature* **246**, 18–22 (1973).
9. R. D. Müller, M. Sdrolias, C. Gaina, B. Steinberger, C. Heine, Long-term sea-level fluctuations driven by ocean basin dynamics. *Science* **319**, 1357–1362 (2008).
10. M. Gurnis, Phanerozoic marine inundation of continents driven by dynamic topography above subducting slabs. *Nature* **364**, 589–593 (1993).
11. P. M. Burgess, M. Gurnis, Mechanisms for the formation of Cratonic stratigraphic sequences. *Earth Planetary Sci. Lett.* **136**, 647–663 (1995).
12. J. X. Mitrovica, C. Beaumont, G. T. Jarvis, Tilting of continental interiors by the dynamical effects of subduction. *Tectonics* **8**, 1079–1094 (1989).
13. W. C. Pitman, Relationship between eustacy and stratigraphic sequences of passive margins. *GSA Bull.* **89**, 1389–1403 (1978).
14. D. B. Rowley, Earth's constant mean elevation: Implication for long-term sea level controlled by oceanic lithosphere dynamics in a Pitman world. *J. Geol.* **125**, 141–153 (2017).
15. C. R. Scotese, PALEOMAP Progress (Report 90-0497, University of Texas at Arlington, Arlington, 1997).

16. A. G. A. G. Smith, "Atlas of Mesozoic and Cenozoic coastlines" in *Atlas of Mesozoic and Cenozoic Coastlines*, (Cambridge University Press, Cambridge, 1994), pp. 0-521–45155-8.
17. D. B. Rowley, Sea level: Earth's dominant elevation-implications for duration and magnitudes of sea level variations. *J. Geol.* **121**, 445–454 (2013).
18. J. M. Husson, S. E. Peters, Nature of the sedimentary rock record and its implications for Earth system evolution. *Emerg. Top. Life Sci.* **2**, 125–136 (2018).
19. S. E. Peters, D. P. Quinn, J. M. Husson, R. R. Gaines, Macrostratigraphy: Insights into cyclic and secular evolution of the earth-life system. *Annu. Rev. Earth Planetary Sci.* **50**, annurev-earth-032320-081427 (2022).
20. S. R. Meyers, S. E. Peters, A 56 million year rhythm in North American sedimentation during the Phanerozoic. *Earth Planetary Sci. Lett.* **303**, 174–180 (2011).
21. S. Liu, D. Nummedal, L. Liu, Migration of dynamic subsidence across the Late Cretaceous United States Western Interior Basin in response to Farallon plate subduction. *Geology* **39**, 555–558 (2011).
22. W. A. Yonkee, A. B. Weil, Tectonic evolution of the Sevier and Laramide belts within the North American Cordillera orogenic system. *Earth-Sci. Rev.* **150**, 531–593 (2015).
23. S. E. Peters, J. M. Husson, Sediment cycling on continental and oceanic crust. *Geology* **45**, 323–326 (2017).
24. P. A. Allen, J. J. Armitage, "Cratonic basins" in *Tectonics of Sedimentary Basins*, C. Busby, A. Azor, Eds. (John Wiley & Sons, Ltd, Chichester, UK, 2012), pp. 602–620.
25. C. M. Marcilly, T. H. Torsvik, C. P. Conrad, Global Phanerozoic sea levels from paleogeographic flooding maps. *Gondwana Res.* **110**, 128–142 (2022).
26. Á. T. Kocsis, C. R. Scotese, Mapping paleocoastlines and continental flooding during the Phanerozoic. *Earth-Sci. Rev.* **213**, 103463 (2021).
27. P. G. DeCelles, K. A. Giles, Foreland basin systems. *Basin Res.* **8**, 105–123 (1996).
28. Moresi Burgess, Modelling rates and distribution of subsidence due to dynamic topography over subducting slabs: Is it possible to identify dynamic topography from ancient strata? Identifying dynamic topography in the ancient record *Basin Res.* **11**, 305–314 (1999).
29. C. R. van Staal, S. M. Barr, J. A. Percival, F. A. Cook, R. M. Clowes, Lithospheric architecture and tectonic evolution of the Canadian Appalachians and associated Atlantic margin. *Tectonic Styles Canada: Lithoprobe Persp.: Geol. Assoc. Can. Special Paper* **49**, 55 (2012).
30. F. Macdonald, J. Ryan-Davis, R. Coish, J. Crowley, P. Karabinos, A newly identified Gondwanan terrane in the northern Appalachian Mountains: Implications for the Taconic orogeny and closure of the Iapetus Ocean. *Geology* **42**, 539–542 (2014).
31. J. V. Strauss *et al*., Orogen transplant: Taconic-Caledonian arc magmatism in the central Brooks Range of Alaska. *Geol. Soc. Am. Bull.* **129**, 649–676 (2017).
32. P. M. Burgess, M. Gurnis, L. Moresi, Formation of sequences in the Cratonic interior of North America by interaction between mantle, eustatic, and stratigraphic processes. *Geol. Soc. Am. Bull.* **109**, 1515–1535 (1997).
33. B. Coakley, M. Gurnis, Far-field tilting of Laurentia during the Ordovician and constraints on the evolution of a slab under an ancient continent. *J. Geophys. Res.: Solid Earth* **100**, 6313–6327 (1995).
34. C. M. Rubin, M. M. Miller, G. M. Smith, Tectonic development of Cordilleran mid-Paleozoic volcano-plutonic complexes; Evidence for convergent margin tectonism in Geological Society of America Special Papers. *Geol. Soc. Am.* **255**, 1–16 (1990).
35. J. K. Mortensen, Pre-Mid-Mesozoic tectonic evolution of the Yukon-Tanana Terrane, Yukon and Alaska. *Tectonics* **11**, 836–853 (1992).
36. M. Colpron, J. L. Nelson, A Palaeozoic Northwest Passage: Incursion of Caledonian, Baltican and Siberian terranes into eastern Panthalassa, and the early evolution of the North American Cordillera. *Geol. Soc. London Special Publ.* **318**, 273–307 (2009).
37. K. Faehnrich *et al*., Pre-mississippian stratigraphic architecture of the Porcupine Shear Zone, Yukon and Alaska, and significance in the evolution of Northern Laurentia. *Lithosphere* **2021**, 7866155 (2021).
38. R. N. Pysklywec, J. X. Mitrovica, Mantle flow mechanisms of epeirogeny and their possible role in the evolution of the Western Canada Sedimentary Basin. *Can. J. Earth Sci.* **37**, 1535–1548 (2000).
39. R. N. Cobbett *et al*., Late Devonian magmatism and clastic deposition in the upper Earn Group (central Yukon, Canada) mark the transition from passive to active margin along western Laurentia. *Can. J. Earth Sci.* **58**, 471–494 (2021).
40. P. H. Cashman, D. M. Sturmer, The Antler Orogeny reconsidered and implications for late Paleozoic tectonics of western Laurentia. *Geology* (2023).
41. U. Kroner, M. Roscher, R. L. Romer, Ancient plate kinematics derived from the deformation pattern of continental crust: Paleo- and Neo-Tethys opening coeval with prolonged Gondwana-Laurussia convergence. *Tectonophysics* **681**, 220–233 (2016).
42. J. P. Hibbard, C. R. van Staal, D. W. Rankin, *Comparative Analysis of the Geological Evolution of the Northern and Southern Appalachian Orogen: Late Ordovician-Permian* (Geological Society of America, 2010).
43. U. Kroner, R. Romer, Two plates – Many subduction zones: The Variscan orogeny reconsidered. *Gondwana Res.* **24**, 298–329 (2013).
44. F. G. Poole, W. J. Perry, R. J. Madrid, R. Amaya-Martínez, Tectonic synthesis of the Ouachita-Marathon-Sonora orogenic margin of southern Laurentia: Stratigraphic and structural implications for timing of deformational events and plate-tectonic model. *Geol. Soc. Am.*, (2005).
45. T. F. Lawton, P. H. Cashman, J. H. Trexler, W. J. Taylor, The late Paleozoic Southwestern Laurentian Borderland. *Geology* **45**, 675–678 (2017).
46. M. R. Cecil *et al*., Early arc development recorded in Permian-Triassic plutons of the northern Mojave Desert region, California, USA. *GSA Bull.* **131**, 749–765 (2019).
47. D. A. Levy, A. V. Zuza, P. J. Haproff, M. L. Odlum, Early Permian tectonic evolution of the Last Chance thrust system: An example of induced subduction initiation along a plate boundary transform. *GSA Bull.* **133**, 1105–1127 (2021).
48. A. Embry, B. Beauchamp, K. Dewing, J. Dixon, *Episodic Tectonics in the Phanerozoic Succession of the Canadian High Arctic and the "10-Million-Year Flood"* (Geological Society of America, 2019), pp. 213–230.
49. S. Liu, D. Nummedal, M. Gurnis, Dynamic versus flexural controls of Late Cretaceous Western Interior Basin, USA. *Earth Planet. Sci. Lett.* **389**, 221–229 (2014).
50. C. Chang, L. Liu, Investigating the formation of the Cretaceous Western Interior Seaway using landscape evolution simulations. *GSA Bull.* **133**, 347–361 (2021).
51. P. G. DeCelles, Late Jurassic to Eocene evolution of the Cordilleran thrust belt and foreland basin system, western U.S.A. *Am. J. Sci.* **304**, 105–168 (2004).
52. S. Danise, S. M. Holland, A sequence stratigraphic framework for the middle to Late Jurassic of the Sundance Seaway, Wyoming: Implications for correlation, basin evolution, and climate change. *J. Geol.* **126**, 371–405 (2018).
53. L. Liu, S. Spasojević, M. Gurnis, Reconstructing Farallon plate subduction beneath North America back to the Late Cretaceous. *Science* **322**, 934–938 (2008).
54. W. Cao, C. T. A. Lee, J. S. Lackey, Episodic nature of continental arc activity since 750 Ma: A global compilation. *Earth Planet. Sci. Lett.* **461**, 85–95 (2017).
55. S. Zahirovic *et al*., Tectonic evolution and deep mantle structure of the eastern Tethys since the latest Jurassic. *Earth-Science Rev.* **162**, 293–337 (2016).
56. F. A. Macdonald, N. L. Swanson-Hysell, Y. Park, L. Lisiecki, O. Jagoutz, Arc-continent collisions in the tropics set Earth's climate state. *Science* **364**, 181–184 (2019).
57. R. M. Flowers, F. A. Macdonald, C. S. Siddoway, R. Havranek, Diachronous development of Great Unconformities before Neoproterozoic Snowball Earth. *Proc. Natl. Acad. Sci. U.S.A.* **117**, 10172–10180 (2020).
58. B. Peak, R. Flowers, F. Macdonald, J. Cottle, Zircon (U-Th)/He thermochronology reveals pre-Great Unconformity paleotopography in the Grand Canyon region, USA. *Geology* **49**, 1462–1466 (2021).
59. C. P. Sturrock, R. M. Flowers, F. A. Macdonald, The late Great Unconformity of the central Canadian shield. *Geochem. Geophys. Geosyst.* **22** (2021).
60. K. E. Karlstrom, J. M. Timmons, *Many Unconformities Make One 'Great Unconformity'* (Geological Society of America, 2012).
61. F. A. Macdonald, W. A. Yonkee, R. M. Flowers, N. L. Swanson-Hysell, *Neoproterozoic of Laurentia* (Geological Society of America, 2023), pp. 331–380.
62. G. C. Bond, N. Christie-Blick, M. A. Kominz, W. J. Devlin, An early Cambrian rift to post-rift transition in the Cordillera of western North America. *Nature* **315**, 742–746 (1985).
63. G. C. Bond, M. A. Kominz, Construction of tectonic subsidence curves for the early Paleozoic miogeocline, southern Canadian Rocky Mountains: Implications for subsidence mechanisms, age of breakup, and crustal thinning. *Geol. Soc. Am. Bull.* **95**, 155 (1984).
64. M. Levy, N. Christie-Blick, Tectonic subsidence of the early Paleozoic passive continental margin in eastern California and southern Nevada. *Geol. Soc. Am. Bull.* **103**, 1590–1606 (1991).
65. R. Witkosky, B. P. Wernicke, Subsidence history of the Ediacaran Johnnie Formation and related strata of southwest Laurentia: Implications for the age and duration of the Shuram isotopic excursion and animal evolution. *Geosphere* **14**, 2245–2276 (2018).
66. T. H. Torsvik, L. R. M. Cocks, *Earth History and Palaeogeography* (Cambridge University Press, Cambridge, 2017).
67. A. Young *et al*., Long-term Phanerozoic sea level change from solid Earth processes. *Earth Planet. Sci. Lett.* **584**, 117451 (2022).
68. N. L. Swanson-Hysell, "The Precambrian paleogeography of Laurentia" in *Ancient Supercontinents and the Paleogeography of Earth* (Elsevier, 2021), pp. 109–153.
69. G. Baby, F. Guillocheau, J. Braun, C. Robin, M. Dall'Asta, Solid sedimentation rates history of the Southern African continental margins: Implications for the uplift history of the South African Plateau. *Terra Nova* **32**, 53–65 (2020).
70. J. Braun, F. Guillocheau, C. Robin, G. Baby, H. Jelsma, Rapid erosion of the Southern African Plateau as it climbs over a mantle superswell: Eroding Southern African plateau. *J. Geophys. Res.: Solid Earth* **119**, 6093–6112 (2014).
71. J. R. Stanley *et al*., Constraining plateau uplift in Southern Africa by combining thermochronology, sediment flux, topography, and landscape evolution modeling. *J. Geophys. Res.: Solid Earth* **126** (2021).
72. Z. Li *et al*., Assembly, configuration, and break-up history of Rodinia: A synthesis. *Precambrian Res.* **160**, 179–210 (2008).
73. P. R. Johnson, An expanding Arabian-Nubian shield geochronologic and isotopic dataset: Defining limits and confirming the tectonic setting of a Neoproterozoic accretionary orogen. *Open Geol. J.* **8**, 3–33 (2014).
74. A. M. C. Şengör, N. Lom, C. Zabcı, G. Sunal, T. Öner, Reconstructing orogens without biostratigraphy: The Saharides and continental growth during the final assembly of Gondwana-Land. *Proc. Natl. Acad. Sci. U.S.A.* **117**, 32278–32284 (2020).
75. L. C. M. De Lira Santos *et al*., Combined Nd isotope systematics and geophysical data constrain the crustal evolution of the disrupted Alto Moxotó Terrane, Borborema Province, Brazil. *Tectonophysics* **848**, 229716 (2023).
76. F. Caxito *et al*., Integration of elemental and isotope data supports a Neoproterozoic Adamastor Ocean realm. *Geochem. Perspect. Lett.* **17**, 6–10 (2021).
77. A. Şengör, B. Natal'in, Phanerozoic analogues of Archaean oceanic basement fragments: Altaid Ophiolites and Ophirags. *Dev. Precambrian Geol.* **13**, 675–726 (2004).
78. P. A. Cawood, Terra Australis Orogen: Rodinia breakup and development of the Pacific and Iapetus margins of Gondwana during the Neoproterozoic and Paleozoic. *Earth-Science Rev.* **69**, 249–279 (2005).
79. S. D. Boger, Antarctica – Before and after Gondwana. *Gondwana Res.* **19**, 335–371 (2011).
80. R. J. Squire, C. J. L. Wilson, Interaction between collisional orogenesis and convergent-margin processes: Evolution of the Cambrian proto-Pacific margin of East Gondwana. *J. Geol. Soc.* **162**, 749–761 (2005).
81. J. Foden, M. A. Elburg, J. Dougherty-Page, A. Burtt, The timing and duration of the Delamerian Orogeny: Correlation with the Ross Orogen and implications for Gondwana assembly. *J. Geol.* **114**, 189–210 (2006).
82. P. A. Cawood, M. R. Johnson, A. A. Nemchin, Early Palaeozoic orogenesis along the Indian margin of Gondwana: Tectonic response to Gondwana assembly. *Earth Planet. Sci. Lett.* **255**, 70–84 (2007).
83. D. C. Zhu *et al*., Cambrian bimodal volcanism in the Lhasa Terrane, southern Tibet: Record of an early Paleozoic Andean-type magmatic arc in the Australian proto-Tethyan margin. *Chem. Geol.* **328**, 290–308 (2012).
84. J. Hassanzadeh *et al*., U-Pb zircon geochronology of late Neoproterozoic-Early Cambrian granitoids in Iran: Implications for paleogeography, magmatism, and exhumation history of Iranian basement. *Tectonophysics* **451**, 71–96 (2008).
85. L. K. Zhang *et al*., Cambrian magmatism in the Tethys Himalaya and implications for the evolution of the Proto-Tethys along the northern Gondwana margin: A case study and overview. *Geol. J.* **54**, 2545–2565 (2019).

86. R. Nance, J. Murphy, R. Strachan, R. D'Lemos, G. Taylor, Late Proterozoic tectonostratigraphic evolution of the Avalonian and Cadomian terranes. *Precambrian Res.* **53**, 41–78 (1991).
87. J. B. Murphy, R. D. Nance, Model for the evolution of the Avalonian-Cadomian belt. *Geology* **17**, 735 (1989).
88. U. Linnemann, F. Pereira, T. E. Jeffries, K. Drost, A. Gerdes, The Cadomian Orogeny and the opening of the Rheic Ocean: The diacrony of geotectonic processes constrained by LA-ICP-MS U-Pb zircon dating (Ossa-Morena and Saxo-Thuringian Zones, Iberian and Bohemian Massifs). *Tectonophysics* **461**, 21–43 (2008).
89. P. Andonaegui *et al*., The last stages of the Avalonian-Cadomian arc in NW Iberian Massif: Isotopic and igneous record for a long-lived peri-Gondwanan magmatic arc. *Tectonophysics* **681**, 6–14 (2016).
90. K. Sundell, F. Macdonald, The tectonic context of hafnium isotopes in zircon. *Earth Planet. Sci. Lett.* **584**, 117426 (2022).
91. A. B. Ronov, The Earth's sedimentary shell (quantitative patterns of its structure, compositions, and evolution): The 20th V.I. Vernadskiy Lecture, March 12, 1978. *Int. Geol. Rev.* **24**, 1313–1363 (1982).
92. K. Karlstrom *et al*., Cambrian Sauk transgression in the Grand Canyon region redefined by detrital zircons. *Nat. Geosci.* **11**, 438–443 (2018).
93. K. Karlstrom *et al*., Redefining the Tonto Group of Grand Canyon and recalibrating the Cambrian time scale. *Geology* **48**, 425–430 (2020).
94. A. K. Ault, R. M. Flowers, S. A. Bowring, Phanerozoic surface history of the Slave craton. *Tectonics* **32**, 1066–1083 (2013).
95. R. M. Flowers, Exploiting radiation damage control on apatite (U-Th)/He dates in Cratonic regions. *Earth Planet. Sci. Lett.* **277**, 148–155 (2009).
96. R. M. Flowers, A. K. Ault, S. A. Kelley, N. Zhang, S. Zhong, Epeirogeny or eustasy? Paleozoic-Mesozoic vertical motion of the North American continental interior from thermochronometry and implications for mantle dynamics. *Earth Planet. Sci. Lett.* **317–318**, 436–445 (2012).
97. N. Pinet, B. P. Kohn, D. Lavoie, The ups and downs of the Canadian Shield: 1- preliminary results of apatite fission track analysis from Hudson Bay region. *Technical Report* **8110** (2016).
98. B. P. Kohn, Visualizing thermotectonic and denudation histories using apatite fission track thermochronology. *Rev. Mineral. Geochem.* **58**, 527–565 (2005).